Materials and Structures (2016) 49:553–562
DOI 10.1617/s11527-014-0519-9

ORIGINAL ARTICLE

Simple and fast porosity analysis of concrete using X-ray computed tomography

Anton du Plessis · Babatunde James Olawuyi · William Peter Boshoff · Stephan Gerhard le Roux

Received: 10 July 2014 / Accepted: 22 December 2014 / Published online: 31 December 2014

Abstract X-ray computed tomography is a well-known technique to measure porosity in materials such as concrete, though this usually involves time consuming scans and complex analysis procedures. Many of these involve custom software or programming procedures. In this paper, a simplified procedure is presented and demonstrated using results obtained from basic procedures with commercial software packages, with minimal image processing. The same sample was subjected to scans ranging from 100 to 5 μm resolutions, demonstrating the multiscale ability of commercial CT scanners. Scans done at typical high-quality conditions (1 h duration) in comparison to very fast scans (5 min) are also presented and it is demonstrated that useful information is still obtained from such lower quality faster scans. This demonstrates the concept that X-ray CT is simple and cost effective for research and industrial applications, not requiring expert 3D image analysis experience, for obtaining useful porosity information within the range of pore sizes resolvable by the technique.

A. du Plessis (✉) · S. G. le Roux
CT Scanner Facility, Central Analytical Facilities, Stellenbosch University, Stellenbosch, South Africa
e-mail: anton2@sun.ac.za

B. J. Olawuyi · W. P. Boshoff
Structural Engineering and Civil Engineering Informatics Unit, Department of Civil Engineering, Stellenbosch University, Stellenbosch, South Africa

Keywords X-ray computed tomography · Pore size distribution · Image analysis

1 Introduction

A recent review article discusses the many potential applications of X-ray CT in materials sciences and the potential of the method for quantitative analysis, especially also for porosity analysis [15]. A good overview of porosity analysis by X-ray CT for materials science applications is also presented in [19]. A report of X-ray tomography of building materials including concrete is given by Bentz et al. [11]. In this work, the authors provide some of the first reported results of synchrotron based X-ray micro tomographic studies of concrete and building materials. Porosity analysis of concrete by X-ray micro CT was also reported by Lu et al. [14]. They studied concrete average porosity and pore connectivity using synchrotron based X-ray tomography at resolutions of 1 and 4 μm. In this work, due to the resolution and hence the smaller field of view of the scans, the aggregates were excluded and hence porosity values were found to be higher than the average expected for the concrete bulk. They created a measure called "disconnected pore distance" which correlates well with permeability even though the resolution is not good enough to image all pores in the samples, since sub-micron sized pores are expected in concrete.

Concrete porosity and its relation to the strength of the material have been studied by mercury intrusion porosimetry (MIP) over a range of resolutions from the macro to the nanoscale by [13]. Concrete porosity was also reviewed by [9] and this work included results from 2D analysis using electron microscopy. In this work, the fractal nature of concrete porosity was presented, which essentially illustrates the effect that the size range of analysis affects the results obtained. Diamond also published a paper [10] on how the widely used method MIP is problematic and can result in entirely incorrect pore size distribution analysis, and he discusses the potential for closed versus open porosity, pores with varying neck sizes, and more. The analysis of concrete by laboratory based X-ray CT was reported by Cnudde et al. [8]. They provide a comparison between mercury MIP and microCT at a resolution of 10 μm with some description of the porosity information gained from microCT for this type of sample, also providing CT images of samples before and after MIP, which allows visualization of the mercury intrusion due to mercury being a very strong X-ray absorber. Taud et al. [21] report a porosity estimation method which overcomes some of the problems with the user-defined thresholding process for image processing from micro CT scans, applied to porosity in rocks. One particular advantage of CT is the ability to scan the same sample under different conditions and monitor changes, as demonstrated by Kim et al. [12] for concrete at elevated temperatures, where the porosity change in the concrete was investigated.

Clearly, X-ray computed tomography has in the last 20 years become a powerful non-destructive test method for porosity and defect analysis of various materials, yet very few simple examples have been reported in the literature. Most reported examples are quite complex as mentioned above and focus on the advantages of 3D analysis such as information on pore connectivity or pore shapes, amongst others. Though complex 3D analyses are interesting and can provide unique information not available in many other analysis methods, it is not widely known that micro CT scans can be done at relatively high speed and throughputs (and hence low cost) providing also more basic information on average porosity and pore size distributions. In this paper a simple and almost automated porosity analysis from a CT scan of a concrete sample is presented. The method is useful for full volumetric analysis of porosity within the range of size scales from the scan resolution to the total field of view of the scan. In the case of a 100 μm resolution scan the field of view is 100 mm, making the method suitable for characterization of pores larger than 200 μm up to a maximum size of 100 mm. By doing higher resolution scans smaller pores can be characterized as well as indicated by multiscale results from scans at a range of resolutions down to 5 μm (with a full field of view of 5 mm). Finally a comparison of slow and fast scans to compare the quality and its effect on porosity analysis results are presented and discussed.

2 Experimental details

The work reported here was carried out towards developing a method for 3D void analysis of high performance concrete (HPC) containing superabsorbent polymer as internal curing agent hence a very low water binder concrete is required. Specifically, a 0.25 water/binder (W/B) HPC was adopted in this study. Mix proportioning for HPC always warrant the use of silica fume and superplasticizer while very low W/B concrete as is the choice in this work calls for use of very coarse sand particles (low dust content) and attention given to the mixing procedure for consistency and good workability [1, 2, 17]. A natural sand with minimum particle size of 300 μm (i.e. all the particles smaller than 300 μm were removed using sieving method) serve as the fine aggregate. It has the following physical properties: fineness modulus (FM = 2.79); coefficient of uniformity ($C_u = 2.43$); coefficient of gradation ($C_c = 1.02$); dust content (0.3 %) and is a medium sand classification [20]. These properties had earlier been reported in [18]. The coarse aggregate used is 13 mm greywacke stone and OPC CEM I 52.5N was the binder with silica fume (SF, 7.5 % b_{woc}), added as cement extender while Premia 310—a PCE (2.75 % b_{woc}) was added as superplasticizer (see Table 1 for detail mix composition).

The fine aggregate was first poured into the 50 litres capacity pan-mixer, followed by the binders which had first been thoroughly hand-mixed to enhance even dispersion of the SF and the other cementitious materials (FA or CS as appropriate) and a uniform colour observed. All the fine contents mixed for another 1 min before the coarse aggregate was added

Table 1 Mix composition of HPC mixture adopted

Constituents	(kg/m^3)
Water	134
Cement (CEM I 52.5N)	540
Coarse aggregate (13 mm maximum)	1,050
Sand (retained on 300 μm sieve)	710
Silica fume	40
Superplasticizer (Chryso Premia 310)	16
Slump flow (mm)	550
Water/binder (*W*/*B*) ratio	0.25

W/*B* = ((water + superplasticizer)/(cement + silica fume))

and mixing continued for another 1 min before water already mixed with superplasticizer (Chryso fluid Premia 310—a PCE) was added and mixing allowed to continue for another 3 min as recommended in literature [1, 16, 17].

Slump flow measurement was then carried out using the flow table test (as described in BS EN 12350 – 5:2009 [4]) as a measure of workability and cohesion of the HPC mixture while both the room and concrete temperature were also measured using a digital pocket thermometer (Checktemp 1, Model No. H1—740024, by HANNA Instruments Incorporated, United States). After ascertaining that the mixture met the required workability and cohesion for specified design mix, specimen for the HPC mixture of 28 day characteristic strength ($f_{ck,\ cube}$) minimum was cast into 50 mm Ø × 100 mm in two layers on a vibrating table into the already oiled moulds. These was thereby covered in the Laboratory with thick polythene sheets and allowed to harden for 24 h before de-moulding and curing in water bath at 20 ± 3 °C till the required curing age of 28 days before testing in accordance to relevant BS Standards – BS EN 12350 [3, 4], BS EN 12390 [5, 6], Eurocode 2 [7].

Dry hardened HPC were then subjected to X-ray CT scans with a General Electric Phoenix VTomeX L240, at the Stellenbosch University CT Scanner Facility. Various scan settings were used at resolutions from 100 to 5 μm. Samples were cast in a cylinder shape for best scanning geometry. The cylindrical geometry allows minimization of beam hardening artefacts due to the X-ray penetration length being equal from all projection angles as the cylinder rotates around its axis in the scan. Fast scans at 100 μm resolution were done at 180 kV and 100 μA, without averaging or skipping of images, 131 ms per image and 1,000 images recorded during one full rotation of the sample. This combination of settings resulted in approximately 3–5 min per scan, excluding sample setup and background detector calibration. Background detector calibration is only necessary once, when large batches of samples are scanned in succession. Additionally, a background detector region of interest is selected which corrects for potential X-ray flux variations. Typical slower scans and scans at higher resolution used the same X-ray generation settings, but increased image acquisition time, numbers of projection images and averaging of images. All scans were performed with a copper filter of 0.6 mm to reduce beam hardening artefacts. Data is reconstructed using system-supplied Datos reconstruction software, which uses a modified Feldkamp algorithm based on filtered backprojection. Offset correction and axis shift corrections are incorporated to ensure high data quality. Clamping is activated in order to generate a higher data depth in the grey values of interest. A background region of interest is used to correct for possible X-ray flux variations.

Reconstructed volumes were analysed with the commercial software package VGStudioMax 2.2 with the defect analysis module. The data is smoothed using a median filter before any analysis, which removes noise. The simplified procedure for obtaining porosity information involves selecting the object (the concrete cylinder) using an adaptive rectangle around the object, and hence removing all air from the 3D data set, not internal to the object. At this step, average void fraction can be calculated using the volume analysis tool. A surface fit function is then applied using the threshold value as the central value between the peak of material and air, in the data histogram. This 3D surface indicates the transition between material and pore. This procedure does have limitations: when data contains peaks which are not well separated (in which case the central value is not simple to find and noise will be inherent) or when peaks are very much separated and noise is present in the scan (in which case noise will be selected as part of the pore volume). These limitations can be overcome when noise is inherently low in the scan, and peaks are separated well enough. The software provides an automated function for finding the central value for threshold and an advanced additional function refines this value by searching the vicinity of the chosen threshold value in

3D for sharpest variation, ensuring the threshold is accurate. The search distance is typically 3 voxels.

Once the surface fit has been applied, a region of interest or mask is created of the pore volume enclosed by the surface. An automated defect analysis is then done using the defect analysis module of VGStudio Max 2.2, using this mask as selection, and limited to a pore size of at least eight voxels in total. This function generates information on each individual pore (unconnected feature) including diameter, volume, surface area, sphericity and more.

The method described above minimizes human error (especially between different scans) and visual confirmation/validation of the accuracy of the selection is possible in 2D slice views. For example, once segmentation is performed, the slice images can be analysed to ensure all pores are selected and that nothing is selected which is not a pore, by switching the segmentation on and off, while scrolling through the volume.

2D analysis was carried out using free image analysis software ImageJ. Slice images were analysed in 2D by selecting material including voids, and calculating void area fractions using a threshold value central between the material and air peaks. A plugin was coded in order to repeat this procedure across a stack of images and thereby generate 2D void area fraction versus distance across the sample, by using the same threshold value in each image.

3 Results and discussions

3.1 Basic analysis

A microCT scan at 100 μm resolution can be done in a relatively short time on this entire sample, down to less than 5 min. An example of such a scan is shown in Fig. 1, with the voids removed and visualized in 3D with a blue colour to the right of the exterior surface view of the concrete cylinder, the average porosity in this example is 3.5 %. This fast method is particularly useful when an interest is specifically in the largest pores. The smallest detected pore diameter is typically double the scan resolution, i.e. 200 μm diameter in this case. Three data histograms are also presented showing the separation between air and material, and the variation between scans of different concrete samples. Each scan therefore needs its own threshold value. Figure 2 shows a slice image and the thresholding operation to calculate void fraction, used for both 2D and 3D void fraction calculations.

The thresholding operation is a manual human interface, which has an inherent error margin based on human perception of the edge of the void region. Additionally, image artefacts can cause errors (for example beam hardening could cause some small voids near the edge of the sample to appear brighter than identical voids in the middle part of the sample, due to a gradual intensity variation across the sample).

Figure 3 shows 2D analysis of the slices from top to bottom through the sample, indicating that the actual porosity variation within the sample is quite large, varying roughly from 2.5 to 5 %. Human error on the measurement would be in the same range using normal thresholding, but the 2D porosity analysis shown in Fig. 3 is without human error as the threshold is maintained across all slices.

The 2D area void fractions vary in a range from 2.5 to 5 %, with an average value of 3.5 %. For the same choice of threshold value, the 3D volumetric void fraction was calculated as 3.25 % in a commercial 3D analysis software package. The slightly different volumetric value can be explained by slightly different subvolumes (top and bottom edges are cropped to eliminate edge artefacts) and other possible causes of difference can arise from the material segmentation from the background or voxel interpolations applied in the software moving from 2D to 3D. The additional information gained from 3D analysis includes 3D void size distribution, for example colour-coding the voids based on their size or volume. This is demonstrated in Fig. 4 with a cropped 3D view for ease of interpretation.

This analysis can be extended in commercial packages to yield 3D void size distribution data (in this case void volume distribution) in the form of a histogram as in Fig. 5, which shows the total void size distribution for a 100 μm resolution scan, where the biggest detected void is 113 mm^3 and the smallest is 0.064 mm^3. The second histogram shows the range of voids in the smaller size range, up to 4 mm^3. The trend indicated that most pores are of the smallest size interval. This indicates that more pores might be missed that are smaller than the resolution, as is expected for concrete.

Besides void size distributions, other information such as void surface area and shape factors can be calculated. One simple calculation is that of sphericity, which is based on a calculation using the 3D void surface area and volume. A plot of sphericity is shown

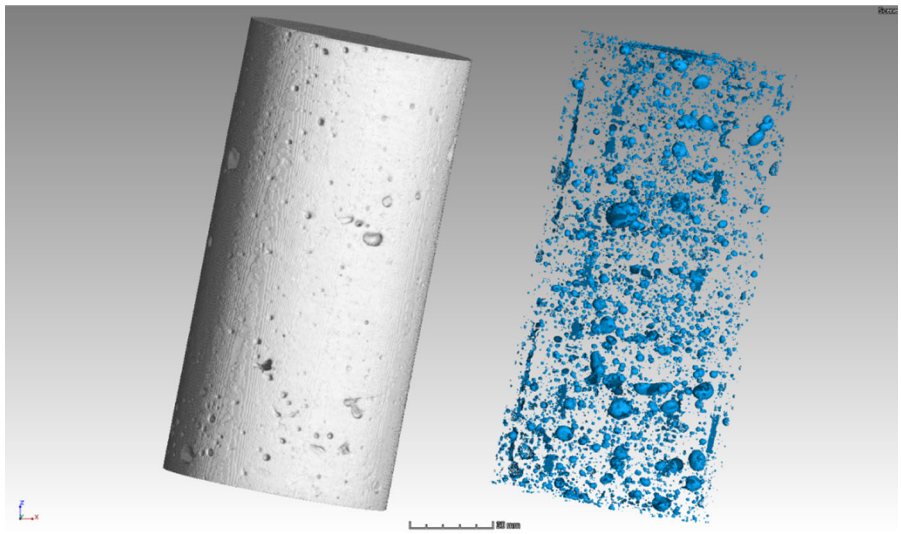

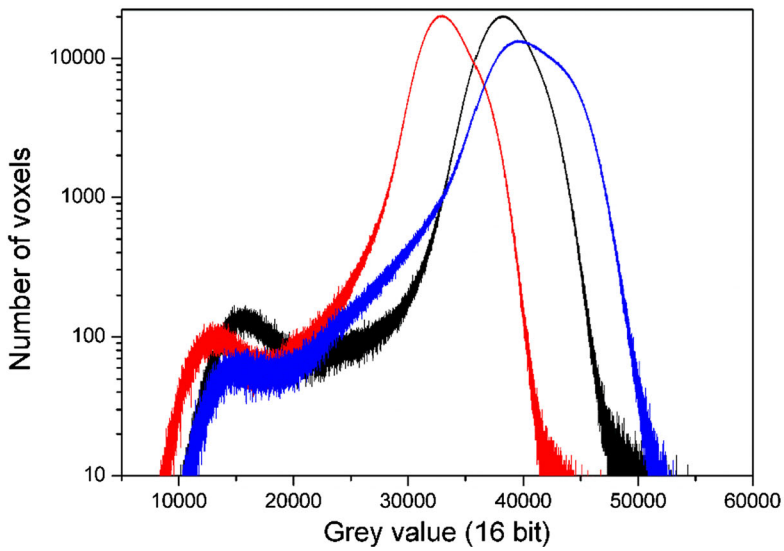

Fig. 1 100 µm scan of concrete core with 3D visualization of porosity in *blue* (*top*) and data histograms representing the voxel *grey* values of three scans of different samples, indicating the separation of air (*left peak*) and material (*right peak*). (Color figure online)

in Fig. 6, indicating that in this case the largest voids are least spherical (perfect sphere = 1). Figure 7 shows the least spherical and most spherical voids in 3D images, clearly also indicating that the largest defects are least spherical and vice versa.

3.2 Multiscale analysis

The same sample was scanned at 100, 60, 40, 20, 10 and 5 µm. The 100 and 60 µm scans contain the same volume while the sample was physically sectioned for higher resolution scans, and the 10 and 5 µm resolution scans were done as "subvolume" scans, in which the sample over-fills the detector screen and hence results in a central subvolume represented in the scan, rather than the entire object of interest. Due to the different resolution scales, not only does the smallest detectable void become smaller, but larger voids cannot be detected as they become too large for the field of view. The smallest detectable void is double the resolution in terms of diameter of a spherical void. Therefore the smallest void detected positively at

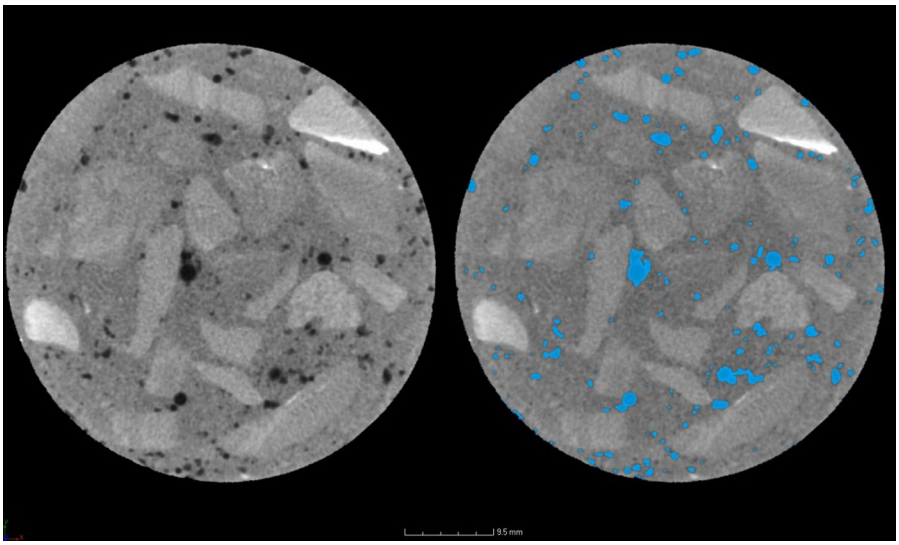

Fig. 2 Thresholding applied to slice image

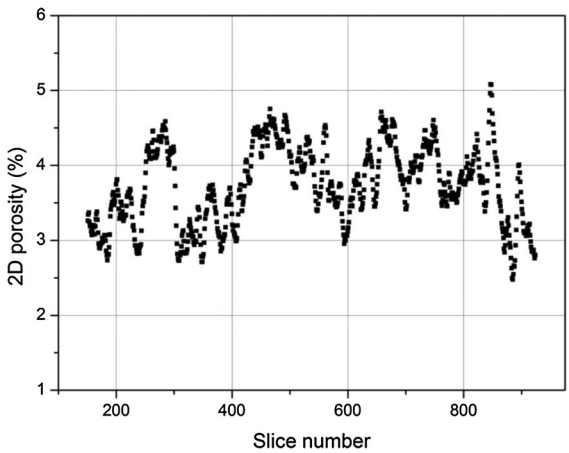

Fig. 3 2D porosity (void area %) from top to bottom of cylindrical sample, excluding the edge regions. Slices at 0.1 mm spacing

100 μm is 200 μm in diameter, and the smallest void in the 5 μm scan is 10 μm in diameter. This is a function of scan quality, and faster scans do not resolve small voids as good quality scans. The combined void size distributions of these scans are shown in Fig. 8. The general trend is that smaller voids are most abundant, even at the highest resolution scan, indicating that even smaller voids are most likely present that are not resolved at 5 μm. It is also clear that as the scale of measurement decreases, the largest void detectable also becomes smaller. This is one of the reasons for studying samples at different scales as demonstrated here. The average volumetric measured porosity at each resolution scale was: 100 μm: 2.4 %; 60 μm: 2.3 %; 40 μm: 2.0 %; 20 μm: 2.0 %; 10 μm: 2.0 %; 5 μm: 2.4 %.

3.3 Fast scans

Of particular interest is the setting up of microCT scan parameters for faster scans, in order to make the technique more cost effective and making it possible to scan larger batches of samples for better statistical information, for example. In Fig. 9, slice images are compared from a typical slow scan (1 h—left) and a fast scan (5 min—right). Both scans were done at 100 μm resolution, but the slower scan acquired more images including averaging and skipping of images, as well as longer image integration time for better signal to noise ratio. Clearly, the image quality is better in the slow scan image, but the question is how this affects porosity measurements.

The average volumetric porosity measurements from these two scans were different, with 3.3 % for the slow scan and 2.5 % for the fast scan. The increased noise in the faster scan images result in potentially some smaller voids not positively included due to less sharp edges, resulting in lower average values. The 2D porosity profiles across the samples are shown in Fig. 10, indicating the same variation in the

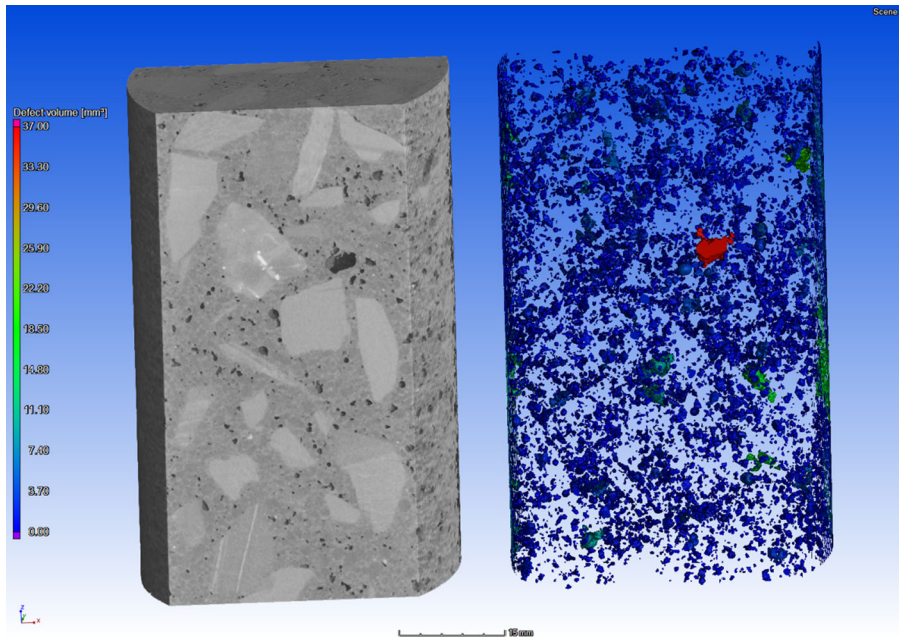

Fig. 4 3D view of cylindrical sample cut open virtually with *colour-coded* voids according to size from the 3D analysis

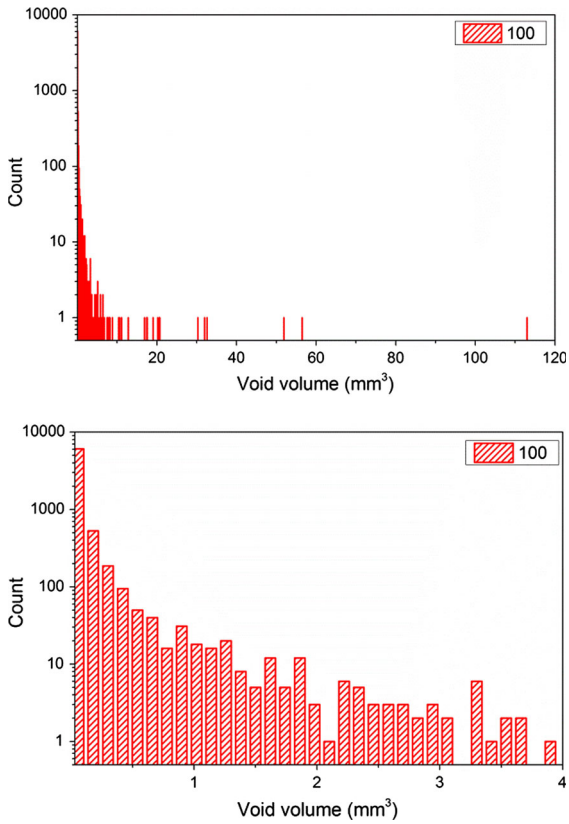

Fig. 5 Histogram of void size distribution for 100 µm scan at two different void size ranges

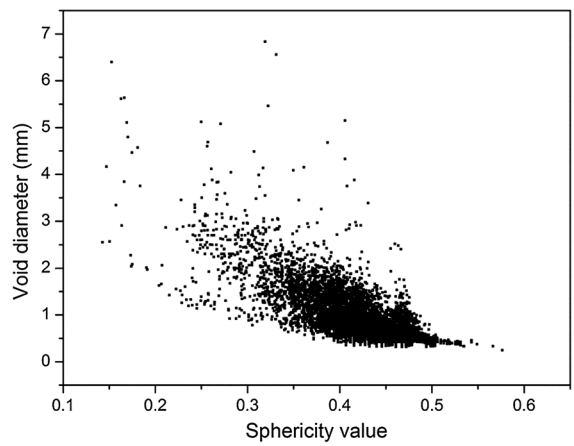

Fig. 6 Void diameter as a function of sphericity, indicating that smaller voids are somewhat more spherical (ideal sphere sphericity value = 1)

measurement but a smaller average porosity value for the faster scan.

The difference in average porosity here can be explained by the presence of many small voids, some of which are detected more easily with a higher quality scan—therefore the detail detectability and effective resolution of the higher quality scan is better. Figure 11 shows a comparison of the void size

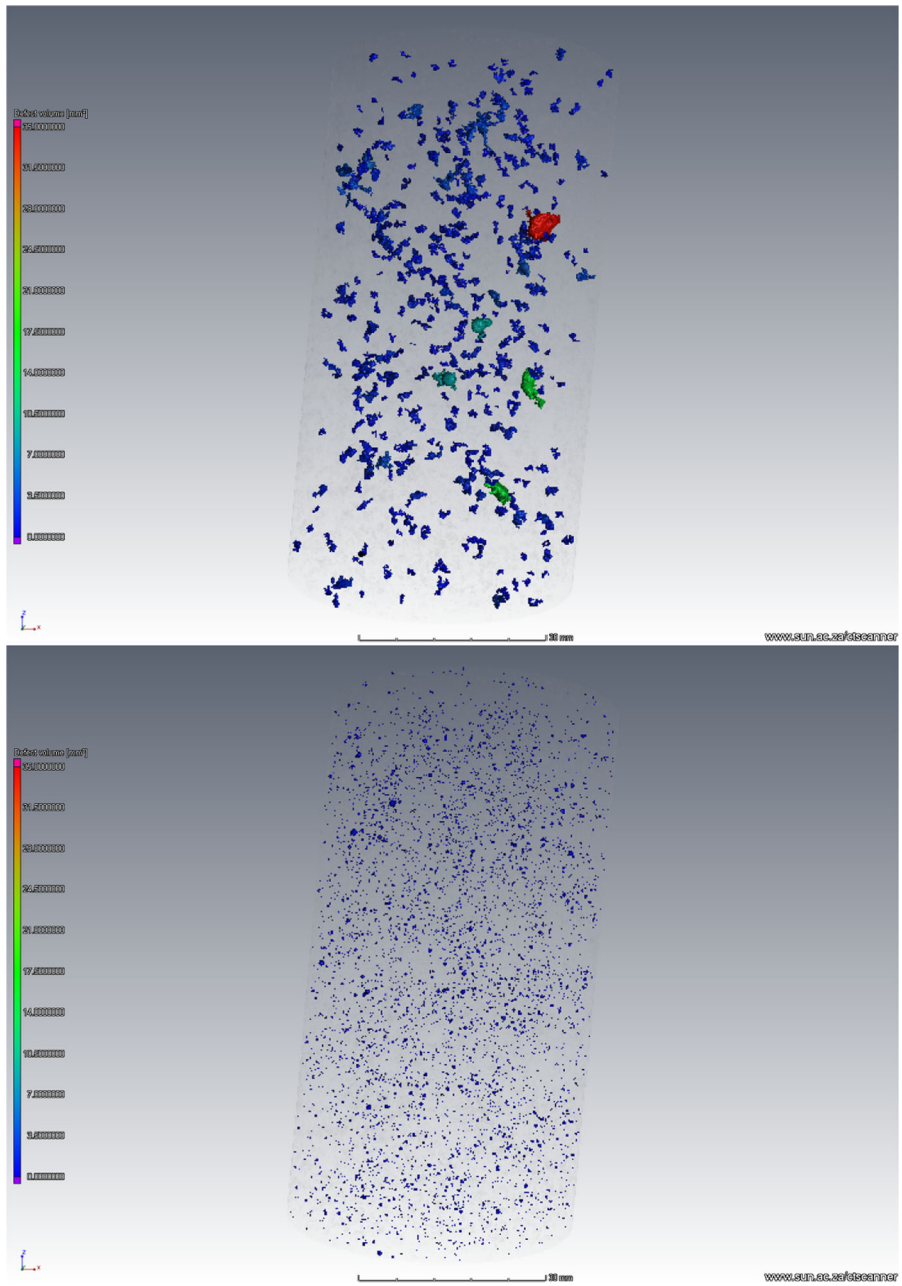

Fig. 7 Selective void visualization of the least spherical (*top*) and most spherical (*bottom*) voids. Clearly the largest-volume voids are also least spherical, and smallest voids are most spherical

distributions of the slow and fast scans, indicating similar results, though the largest void is measured slightly smaller in the faster scan. This can be explained by a less well defined edge and therefore a difference in the threshold value and hence measured volume. It can also be noticed that in the first three intervals, the number of detected pores is higher in the higher quality scan, thereby contributing to the higher average porosity measurement.

4 Discussion and conclusions

The method of porosity analysis from CT data was demonstrated on a simple sample with suitable geometry which minimized image artefacts and allows fast scan times to be possible. The segmentation procedure is followed by 2D or 3D analysis of void area or volume fraction (average porosity) as well as porosity versus distance and volumetric porosity

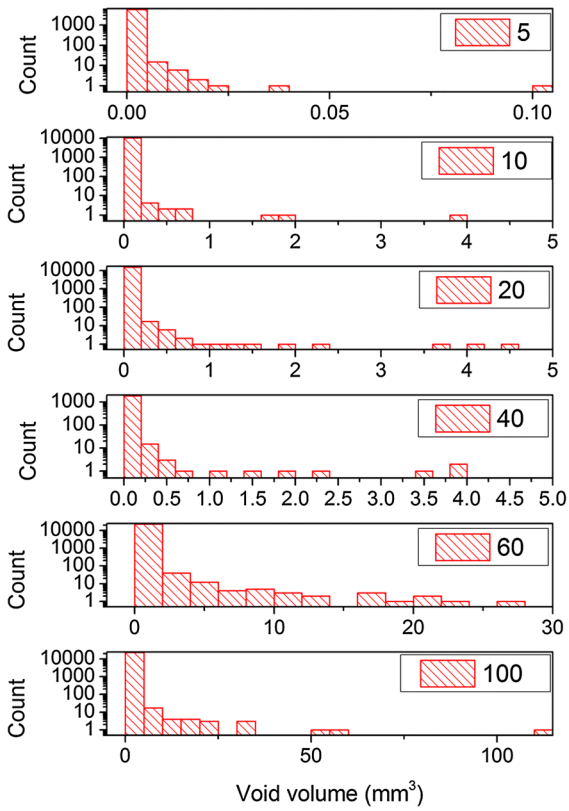

Fig. 8 Histograms of void size distributions of the same sample from scans ranging from 100 to 5 μm resolution

analysis. The 2D porosity versus distance gives an indication of the variation of porosity within a sample, and can be useful if there are variations from one side to the other. The 3D analysis allows void size

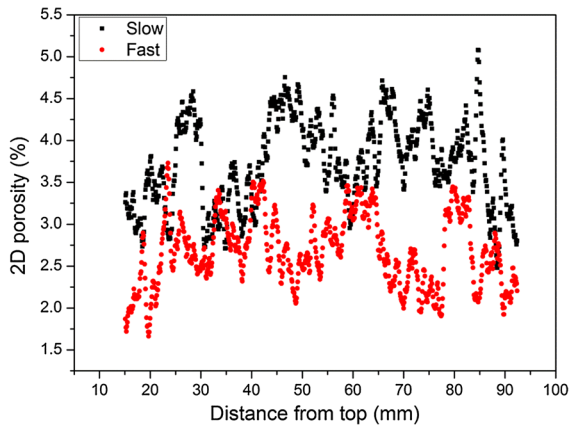

Fig. 10 Comparison of 2D porosity values for slow and fast scans

distribution with colour coding, visual inspection of selected voids, as well as categorization of voids. In this case the result is clear that smaller voids than the scan resolution are still present in the sample. Using the sphericity value or other more complex calculations, potentially voids can be classified and separated according to their origin (e.g. elongated voids along aggregate stones vs spherical voids). The potential of commercial CT scanners to image the same sample at multiple scales of interest (fields of view and resolutions) was demonstrated from 100 μm (FOV approx. 100 mm) to 5 μm (FOV approx. 5 mm). The higher the resolution, the smaller the detected voids. The potential for higher throughput by faster scanning was investigated and it was found that useful porosity

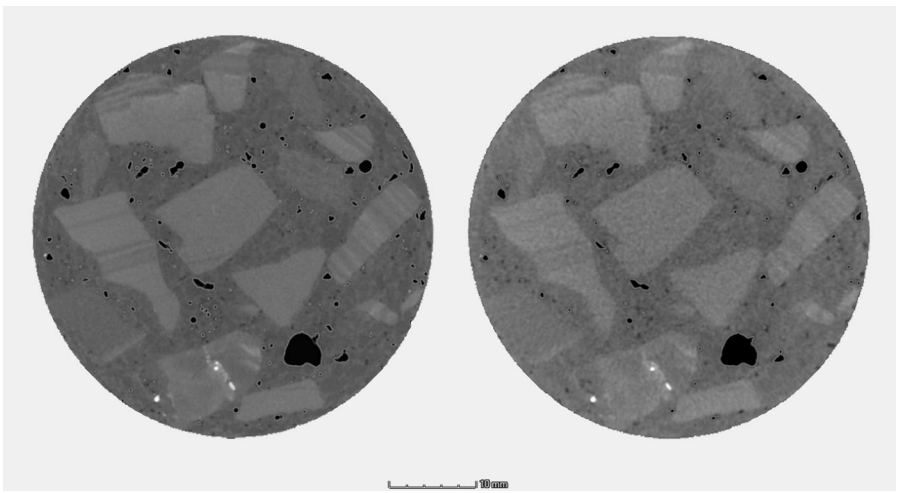

Fig. 9 Slice images of slow (*left*) versus fast (*right*) scan parameters

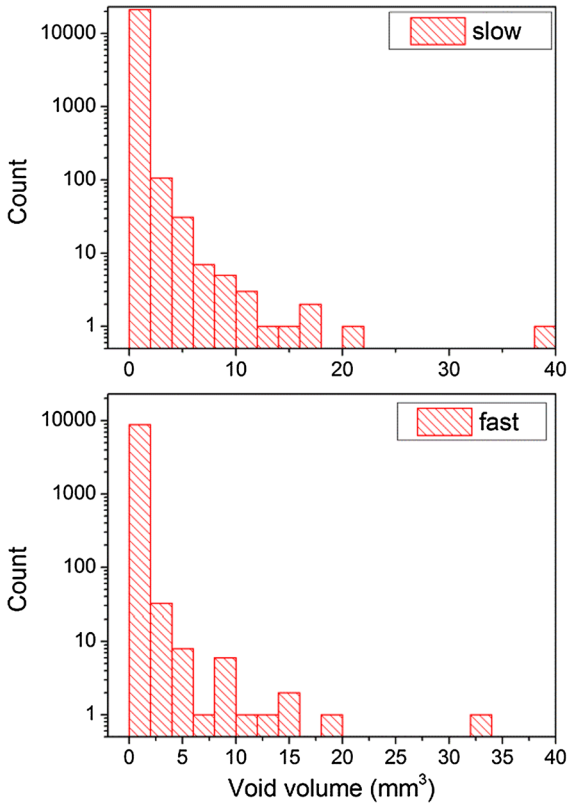

Fig. 11 Comparison of slow versus fast scan on the void size distribution histogram

values could be found at scan times of 5 min, comparable with longer higher quality scans. One difference is that the average porosity measurement is decreased due to lower image quality, mainly due to increased noise and some pores small pores not segmented properly. The size distribution histogram is very similar and good data interpretation is possible, especially when large pores of interest and large batches of samples need to be compared to one another.

Acknowledgments Jakob Petren is acknowledged for 2D analysis support with ImageJ.

References

1. Aïtcin PC (1998) High-performance concrete. Taylor & Francis, London
2. Beushausen H, Dehn F (2009) High-performance concrete. In: Owens G (ed) Fulton's concrete technology, 9th edn. Cement and Concrete Institute, Midrand, pp 297–304
3. British Standards Institution (2000) Testing of fresh concrete, BS EN 12350: part 1, sampling. BSI, London
4. British Standards Institution (2000) Testing of fresh concrete, BS EN 12350: part 5, flow table test. BSI, London
5. British Standards Institution (2000) Testing of hardened concrete, BS EN 12390: part 1, shape, dimension and other requirement for specimens and mould. BSI, London
6. British Standards Institution (2000) Testing of hardened concrete, BS EN 12390: part 2, making and curing specimen for strength tests. BSI, London
7. British Standards Institution (2004) Eurocode 2: design of concrete structures—part 1-1: general rules. 1. British Standard Institution (BSI), London
8. Cnudde V, Cwirzen A, Masschaele B, Jacobs P (2009) Porosity and microstructure characterization of building stones and concretes. Eng Geol 103(3):76–83
9. Diamond S (1999) Aspects of concrete porosity revisited. Cem Concr Res 29(8):1181–1188
10. Diamond S (2000) Mercury porosimetry: an inappropriate method for the measurement of pore size distributions in cement-based materials. Cem Concr Res 30(10):1517–1525
11. Bentz DP, Halleck PM, Grader, AS, Roberts JW (2006) Four-dimensional X-ray microtomography study of water movement during internal curing. In: Proceedings of the international RILEM conference—volume changes of hardening concrete: testing and mitigation, pp 11–20
12. Kim KY, Yun TS, Park KP (2013) Evaluation of pore structures and cracking in cement paste exposed to elevated temperatures by X-ray computed tomography. Cem Concr Res 50:34–40
13. Kumar R, Bhattacharjee B (2003) Porosity, pore size distribution and in situ strength of concrete. Cem Concr Res 33(1):155–164
14. Lu S, Landis E, Keane D (2006) X-ray microtomographic studies of pore structure and permeability in Portland cement concrete. Mater Struct 39(6):611–620
15. Maire E, Withers PJ (2014) Int Mater Rev 59(1):1–43. doi:10.1179/1743280413Y.0000000023
16. Mehta PK, Monteiro JM (2014) Concrete microstructure properties and materials, 4th edn. McGraw-Hill Education, New York. ISBN: 978-0-07-179787-0; MHID: 0-07-179787-4
17. Neville AM (2012) Properties of concrete, 5th edn. Pearson Educational Limited, Essex. ISBN 978-0-273-75580-7
18. Olawuyi BJ, Boshoff WP (2013) Influence of particle size distribution on compressive strength and elastic modulus of high performance concrete. In: International conference on Advances in cement and concrete technology in Africa (ACCTA, 2013), Johannesburg, pp 825–833
19. Salvo L, Cloetens P, Maire E, Zabler S, Blandin J, Buffière J, Ludwig W, Boller E, Bellet D, Josserond C (2003) X-ray micro-tomography an attractive characterisation technique in materials science. Nucl Instrum Methods Phys Res Sect B 200:273–286
20. Shetty MS (2004) Concrete technology—theory and practice. S. Chand and Company Limited, New Delhi
21. Taud H, Martinez-Angeles R, Parrot J, Hernandez-Escobedo L (2005) Porosity estimation method by X-ray computed tomography. J Petrol Sci Eng 47(3):209–217